



Search for the Higgs boson
in $H \rightarrow WW^* \rightarrow ll'$ ($l, l' = e, \mu$) decays with 1.7 fb^{-1} of data at DØ

The DØ Collaboration
URL <http://www-d0.fnal.gov>
(Dated: November 28, 2007)

A search for the Higgs boson is presented using $H \rightarrow WW^* \rightarrow ll'$ ($l, l' = e, \mu$) decays in $p\bar{p}$ collisions at a center-of-mass energy of $\sqrt{s} = 1.96 \text{ TeV}$. Final states containing either two electrons (e^+e^-), an electron and a muon ($e^\pm\mu^\mp$) or two muons ($\mu^+\mu^-$) have been considered. The data sample used in this analysis has been collected between April 2002 and May 2007 by the DØ detector at the Fermilab Tevatron collider, corresponding to an integrated luminosity of approximately 1.1 fb^{-1} in the e^+e^- , $e^\pm\mu^\mp$ and $\mu^+\mu^-$ final states for Run IIa and of 0.6 fb^{-1} for the $\mu^+\mu^-$ final state for Run IIb. No significant excess above the Standard Model background has been observed and upper limits on the production cross section times branching ratio $\sigma \times BR(H \rightarrow WW^*)$ are presented for the combination of the three channels using the Run II dataset of 1.7 fb^{-1} .

I. INTRODUCTION

In the Standard Model (SM) the Higgs boson is crucial to the understanding of electroweak symmetry breaking and the mass generation of electroweak gauge bosons and fermions. Direct searches at the CERN e^+e^- collider (LEP) yielded a lower limit for the Higgs boson mass of $m_H > 114.4$ GeV [1] at 95% CL. Indirect measurements via fits to the electroweak precision data give an upper bound of $m_H < 166$ GeV [2] at 95% CL.

In this note a search for Higgs bosons decaying to the WW^* final state in the DØ experiment at the Tevatron is presented. To achieve a good signal-to-background ratio, the leptonic decay modes $H \rightarrow WW^* \rightarrow ll'$ ($l, l' = e, \mu$) are considered, leading to final states with two leptons and missing transverse momentum. This decay mode provides the largest sensitivity for the Standard Model Higgs boson search at the Tevatron at a mass of $M_H \sim 160$ GeV [3–5]. This decay mode increases the sensitivity for Higgs boson searches in the intermediate mass region $M_H \sim 130$ GeV if combined with searches exploiting the WH and ZH associated production.

A search with 300 pb^{-1} of Run IIa data has been already published in Ref.[6]. Preliminary results using a cut-based approach using 950 pb^{-1} of Run IIa data can be found in Refs.[7, 8]. The present analysis updates the cut-based approach and compliments it with a Neural Network-based selection using the largest available DØ dataset. Upper limits on the production cross section times branching ratio $\sigma \times BR(H \rightarrow WW^*)$ are presented using the combination of the e^+e^- , $e^\pm\mu^\mp$ and $\mu^+\mu^-$ final states for Run IIa and of the $\mu^+\mu^-$ final state for Run IIb. Finally, results presented in this note are also combined with the $e^\pm\mu^\mp$ [9] and e^+e^- [10] Run IIb upper limits.

II. THE DØ DETECTOR

We briefly describe the main components of the DØ Run II detector [12] that are important to this analysis. The central tracking system consists of a silicon microstrip tracker (SMT) and a central fiber tracker (CFT), both located within a 2.0 T axial magnetic field. The SMT strips have a typical pitch of 50–80 μm and the design is optimized for tracking and vertexing over the pseudorapidity range $|\eta| < 3$, where $\eta = -\ln(\tan \frac{\theta}{2})$ with polar angle θ . The system has a six-barrel longitudinal structure, with each barrel a set of four silicon layers arranged axially around the beam pipe, interspersed with sixteen radial disks. The CFT has eight thin coaxial barrels, each supporting two doublets of overlapping scintillating fibers of 0.835 mm diameter, one doublet parallel to the beam axis, the other tilted by $\pm 3^\circ$ relative to the beam axis. A liquid-argon/uranium calorimeter surrounds the central tracking system and consists of a central calorimeter (CC) covering up to $|\eta| \approx 1.1$ and two end calorimeters (EC) extending coverage to $|\eta| < 4.2$, each housed in separate cryostats [13]. Scintillators between the CC and EC cryostats provide additional sampling of showers for $1.1 < |\eta| < 1.4$. The muon system is located outside the calorimeters and consists of a layer of tracking detectors and scintillation trigger counters inside iron toroid magnets which provide a 1.8 T magnetic field, followed by two similar layers behind the toroid. Tracking in the muon system for $|\eta| < 1$ relies on 10 cm wide drift tubes [13], while 1 cm mini-drift tubes are used for $1 < |\eta| < 2$ [14].

III. DATA AND MC SAMPLES

The data sample used in this analysis has been collected between April 2002 and February 2006 (“Run IIa”) and between June 2006 and April 2007 (“Run IIb”) with the DØ detector at the Fermilab Tevatron collider at $\sqrt{s} = 1.96$ TeV. The integrated luminosity is about 1.1 fb^{-1} in the e^+e^- , $e^\pm\mu^\mp$ and $\mu^+\mu^-$ final states for Run IIa and about 0.6 fb^{-1} in the $\mu^+\mu^-$ final state for Run IIb. For the e^+e^- and $\mu^+\mu^-$ final states the “effective integrated luminosity” is a factor that scales the NNLO $Z/\gamma^* \rightarrow l^+l^-$ ($l = e, \mu$) cross section (see Fig. 1) to the data in the mass region $60 \text{ GeV} < M_{\ell\ell} < 130 \text{ GeV}$. For the $e^\pm\mu^\mp$ final state, the data sample size is determined by normalizing the electron-muon invariant mass distribution to the NNLO $Z/\gamma^* \rightarrow \tau\tau$ cross section (see Fig. 1). Data/MC electron and muon correction factors (trigger, lepton and track reconstruction efficiencies) have been applied to MC before normalization to $Z/\gamma^* \rightarrow ll$. Using this normalization procedure the limit on the $H \rightarrow WW^* \rightarrow ll'$ ($l, l' = e, \mu$) cross section is calculated relative to the NNLO $Z/\gamma^* \rightarrow ll$ cross section. Systematic uncertainties coming from the luminosity determination and data-to-MC correction factors are cancelled by using such a normalization procedure.

All Higgs signals have been generated with PYTHIA 6.323 [15] using the CTEQ6L1 leading order parton distribution functions, followed by a detailed GEANT-based [16] simulation of the DØ detector. The signal cross sections are normalized to the next-to-next-to-logarithmic order (NNLL) calculations [17, 18] and branching ratios are calculated using HDECAY [19]. We consider the Higgs boson production both through gluon-gluon fusion and vector-boson fusion processes at the Tevatron.

The $Z/\gamma \rightarrow ll$ cross section is calculated with CTEQ6 PDFs as $\sigma(Z/\gamma \rightarrow ll) = \sigma_{LO} \times K_{QCD}(Q^2)$, with the LO cross section given by PYTHIA using a LO PDF, whereas the K -factor K_{QCD} is computed at NNLO [20] using a

NLO PDF. The cross section times branching ratio for $Z/\gamma \rightarrow ll$ production in the invariant mass region $60 \text{ GeV} < M_{ll} < 130 \text{ GeV}$ is $\sigma \times BR = 241.6 \text{ pb}$. The $W \rightarrow e\nu$ background level is calculated with NNLO corrections and CTEQ6.1M as listed in Ref. [20]. For inclusive W boson production with decays into a single lepton flavor state this value is $\sigma \times BR = 2583 \text{ pb}$. The calculations of Ref. [21] are used for $t\bar{t}$ production with $\sigma \times BR = 0.076 \text{ pb}$ with single flavor lepton decays of both W bosons. The NLO WW , WZ and ZZ production cross section values are taken from Ref. [22] with $\sigma \times BR = 0.15 \text{ pb}$ for WW , $\sigma \times B = 0.014 \text{ pb}$ for WZ and $\sigma \times BR = 0.002 \text{ pb}$ for ZZ production with decay into a single lepton flavor state. The background due to multi-jet production, when a jet is misidentified as a lepton, is determined from the data using a sample of like-sign di-lepton events with inverted lepton quality cuts (defined as QCD fakes in figure captions).

IV. LEPTON IDENTIFICATION

The $H \rightarrow WW^* \rightarrow ll'$ ($l, l' = e, \mu$) candidates are selected using a three level trigger system. The first trigger level uses hardware to select electron candidates based on energy deposition in the electromagnetic part of the calorimeter and selects muon candidates formed by hits in two layers of the muon scintillator system. Digital signal processors in the second trigger level form muon track candidate segments defined by hits in the muon drift chambers and scintillators. At the third level, software algorithms running on a computing farm and exploiting the full event information are used to make the final selection of events which are recorded for offline analysis. A combination of single lepton, lepton plus track and di-lepton triggers has been used to select e^+e^- , $e^\pm\mu^\mp$, $\mu^\pm\mu^\mp$ final states and ensures a trigger efficiency of $\epsilon_{\text{trig}} > 95\%$.

In the offline analysis electrons are identified by clusters of energy in the electromagnetic calorimeter. These showers are chosen by comparing the longitudinal and transverse shower profiles to those of simulated electrons. The clusters must be isolated, deposit most of their energy in the electromagnetic part of the calorimeter (“em-fraction”), and satisfy a likelihood criterion that includes a spatial track match and, in the CC region, an E/p requirement, where E is the energy of the calorimeter cluster and p is the momentum of the track. All electrons are required to be in the pseudorapidity range $|\eta| < 3.0$. The electron likelihood is used to further enhance the purity of the electron sample by reducing the rate of jets misidentified as electrons. In order to exploit differences in background composition as a function of the Higgs boson mass and to suppress significant backgrounds from W +jets and $W\gamma$, the following electron ID criteria have been applied for e^+e^- final state: tight isolated electrons (“em-fraction” > 0.9 , isolation < 0.2 , likelihood > 0.85) for $M_H < 160 \text{ GeV}$ and loose isolated electrons (“em-fraction” > 0.9 , isolation < 0.2 , likelihood > 0.2) for $M_H \geq 160 \text{ GeV}$.

Muon tracks are reconstructed from hits in the wire chambers and scintillators in the muon system and must match a track in the central tracker. Muon detection is restricted to the coverage of the muon system, i.e. $|\eta| < 2.0$. Muons from cosmic rays are rejected by requiring a timing criterion on the hits in the scintillator layers as well as applying restrictions on the position of the muon track with respect to the primary vertex. To select isolated muons in the $e^\pm\mu^\mp$ final state, the scalar sum of the transverse momentum of all tracks, other than that of the muon, in a cone of $\mathcal{R} = 0.4$ around the muon track must be $E_{\text{trk}}^{\text{iso}} < 2.5$ (4.0) GeV for $M_H < 160 \text{ GeV}$ ($M_H \geq 160 \text{ GeV}$) respectively, where $\mathcal{R} = \sqrt{(\Delta\phi)^2 + (\Delta\eta)^2}$ and ϕ is the azimuthal angle. In addition, the transverse energy deposited in the calorimeter in a hollow cone around the muon is required to be $E_{\text{cal}}^{\text{iso}} < 2.5$ (4.0) GeV for $M_H < 160 \text{ GeV}$ ($M_H \geq 160 \text{ GeV}$) respectively. For the $\mu^+\mu^-$ final state, the leading muon must be isolated both in the tracker and the calorimeter with $E_{\text{trk}}^{\text{iso}} < 4.0 \text{ GeV}$ and $E_{\text{cal}}^{\text{iso}} < 4.0 \text{ GeV}$. The next-to-leading muon must fulfill a p_T -dependent calorimeter isolation criteria.

V. SELECTION STRATEGY FOR THE $H \rightarrow WW^* \rightarrow ll'$ ($l, l' = e, \mu$) FINAL STATE

The decay of two W bosons into electrons or muons results in three different final states $e^+e^- + X$ (ee channel), $e^\pm\mu^\mp + X$ ($e\mu$ channel), and $\mu^+\mu^- + X$ ($\mu\mu$ channel), each of which consists of two oppositely charged isolated leptons with high transverse momentum, p_T , and large missing transverse energy, \cancel{E}_T , due to the escaping neutrinos. The analysis sensitivity can be improved by using selection requirements which depend on the Higgs mass, thereby reflecting the changing kinematics [3]. The list of the mass dependent cuts are given in Table I for the e^+e^- , $e^\pm\mu^\mp$ final states and in Table II for the $\mu^+\mu^-$ channel.

In all three final states, two leptons originating from the same vertex are required to be of opposite charge, and must have $p_T^e > 15 \text{ GeV}$ for the leading electron and $p_T^\nu > 10 \text{ GeV}$ for the trailing one in the e^+e^- channel, $p_T^e > 15 \text{ GeV}$ for the electron and $p_T^\mu > 10 \text{ GeV}$ for the muon in the $e^\pm\mu^\mp$ channel, and $p_T^\mu > 20 \text{ GeV}$ for the leading muon and $p_T^\mu > 10 \text{ GeV}$ for the trailing one in the $\mu^+\mu^-$ final state. In addition, the di-lepton invariant mass is required to exceed 15 GeV for the e^+e^- and $e^\pm\mu^\mp$ final states and 17 GeV for the $\mu^+\mu^-$ final state. Finally, to remove possible

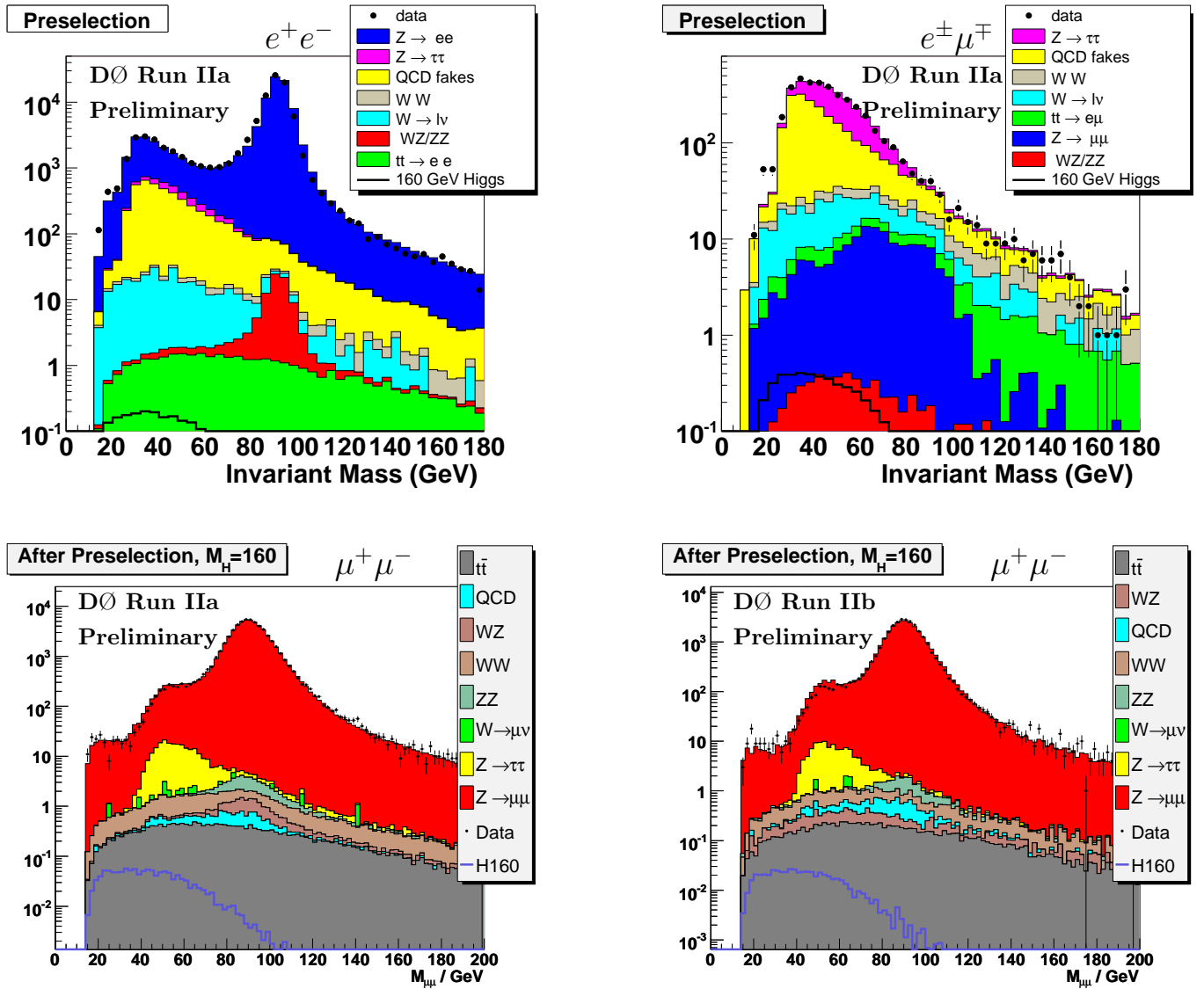


FIG. 1: Distribution of the invariant mass M_{ll} after the initial transverse momentum and di-lepton invariant mass cuts (“Cut 1”, preselection) for the e^+e^- Run IIa (top left), $e^\pm\mu^\mp$ Run IIa (top right), $\mu^+\mu^-$ Run IIa (bottom left) and $\mu^+\mu^-$ Run IIb (bottom right) final states. The expected signal for the Standard Model Higgs of mass 160 GeV is also shown.

contributions from WZ decays in $e^\pm\mu^\mp$ channel, events are vetoed if two electrons or two muons are found in the event and their invariant mass is larger than 70 GeV. These cuts are referred as “Cut 1” (preselection).

The distributions of the invariant mass of the di-lepton system and the missing transverse energy after “Cut 1” (preselection) are shown in Figs. 1 and 2, respectively. The comparison between data and Monte Carlo (MC) are shown separately for the e^+e^- , $e^\pm\mu^\mp$ and $\mu^+\mu^-$ final states in Run IIa and for the $\mu^+\mu^-$ final state in Run IIb.

In all channels the background is largely dominated by Z/γ^* production which is suppressed by requiring the missing transverse energy \cancel{E}_T to be larger than 25-35 GeV. Events are further removed if the \cancel{E}_T could have been produced by a mis-measurement of jet energies, using the following procedure. The fluctuation in the measurement of jet energy in the transverse plane can be approximated by $\Delta E^{\text{jet}} \cdot \sin \theta^{\text{jet}}$ where ΔE^{jet} is proportional to $\sqrt{E^{\text{jet}}}$. The opening angle $\Delta\phi(\text{jet}, \cancel{E}_T)$ between this projected energy fluctuation and the missing transverse energy provides a measure of the contribution of the jet to the missing transverse energy. The scaled missing transverse energy defined as

$$\cancel{E}_T^{\text{Scaled}} = \frac{\cancel{E}_T}{\sqrt{\sum_{\text{jets}} (\Delta E^{\text{jet}} \cdot \sin \theta^{\text{jet}} \cdot \cos \Delta\phi(\text{jet}, \cancel{E}_T))^2}} \quad (1)$$

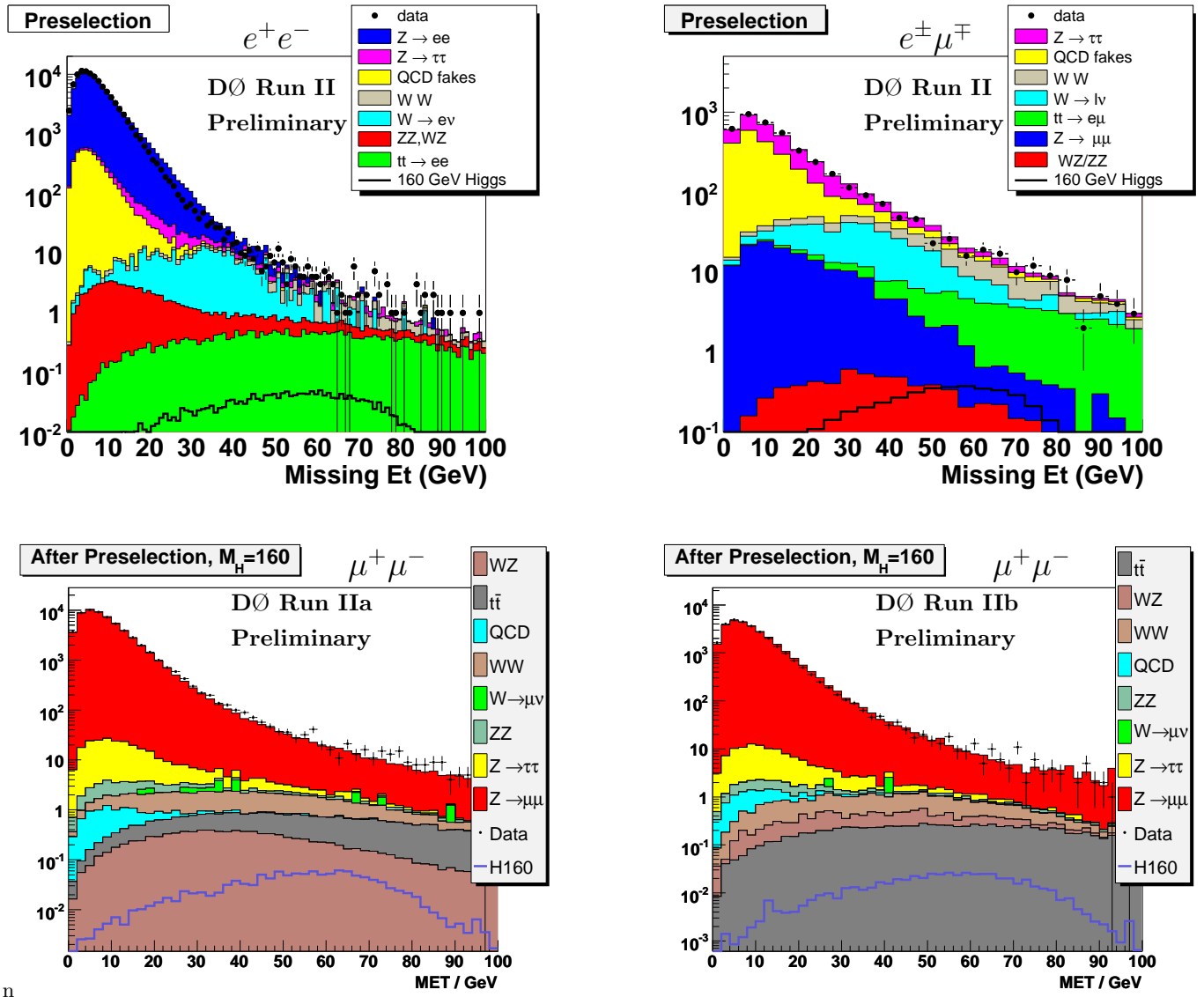


FIG. 2: Distribution of the missing transverse energy \cancel{E}_T after the initial transverse momentum and di-lepton invariant mass cuts (“Cut 1”, preselection) for the e^+e^- Run IIa (top left), $e^\pm\mu^\mp$ Run IIa (top right), $\mu^+\mu^-$ Run IIa (bottom left) and $\mu^+\mu^-$ Run IIb (bottom right) final states. The expected signal for the Standard Model Higgs of mass 160 GeV is also shown.

is required to be greater than 7 (5) for the e^+e^- , $e^\pm\mu^\mp$ ($\mu^\pm\mu^\mp$) final states.

The cuts on the invariant mass of the dilepton system, the opening angle between the leptons in the transverse plane $\Delta\phi_{\ell\ell}$, the sum of the lepton transverse momenta and the missing transverse energy, and on the minimal transverse mass between the lepton and the missing transverse energy are M_H -dependent and optimized differently for e^+e^- , $e^\pm\mu^\mp$ and $\mu^\pm\mu^\mp$ channels to further suppress contributions from Z/γ^* , *diboson*(WW, WZ, ZZ) and $W \rightarrow l\nu$ backgrounds. Since the charged lepton system and the two neutrinos are emitted back-to-back, the invariant mass for the Higgs decays is restricted to approximately $M_H/2$. Thus, depending on the Higgs mass M_H the invariant mass M_{ll} is required to be smaller than this value. The sum of the lepton transverse momentum p_T and the missing transverse energy \cancel{E}_T is required to be approximately in the range $M_H/2 + 20 \text{ GeV} < p_T^l + p_T^{\bar{l}} + \cancel{E}_T < M_H$ in the $\mu\mu$ channel. The minimal transverse energy $M_{min}^T(l, \cancel{E}_T)$ between lepton and \cancel{E}_T in the event $M_T(l, \cancel{E}_T) = \sqrt{2p_T^l \cancel{E}_T (1 - \cos \Delta\phi(l, \cancel{E}_T))}$ is required to be larger than 30 - 75 GeV depending on the Higgs mass and final state in order to suppress background where the \cancel{E}_T is a result of mis-measured lepton momentum. $t\bar{t}$ events are further rejected by a requirement on the scalar sum of the p_T of jets in the event, H_T . Finally a Neural Network (NN) is used to distinguish signal from background.

Selection criterion	Value
Cut 1 Preselection	Trigger, two leptons with opposite charge and $p_T' > 15$ GeV and $p_T^{\prime\prime} > 10$ GeV, $m_{ll} > 15$ GeV ($e\mu$: remove events with $2e$ or 2μ , if $M_{ll} > 70$ GeV)
Cut 2 Missing transverse energy \cancel{E}_T	$\cancel{E}_T > 25$ GeV
Cut 3 $\cancel{E}_T^{\text{Scaled}}$	$\cancel{E}_T^{\text{Scaled}} > 7$ (for $N_{Jet} > 0$)
Cut 4 Invariant mass $M_{ll'}$	$M_{ee} < \min(M_H/2, 80)$ GeV $M_{e\mu} < M_H/2$ GeV
Cut 5 $M_{min}^T(l, \cancel{E}_T)$	$M_{min}^T(l, \cancel{E}_T) > 50$ GeV ($M_H = 120$ GeV) $M_{min}^T(l, \cancel{E}_T) > 55$ GeV ($M_H = 140$ GeV) $M_{min}^T(l, \cancel{E}_T) > 65$ GeV ($M_H = 160$ GeV) $M_{min}^T(l, \cancel{E}_T) > 75$ GeV ($M_H = 180$ GeV) $M_{min}^T(l, \cancel{E}_T) > 65$ GeV ($M_H = 200$ GeV)
Cut 6 Lepton opening angle $\Delta\phi_{ll'}$	$\Delta\phi_{ll'} < 1.25(ee); 1.5(e\mu)$ ($M_H = 120$ GeV) $\Delta\phi_{ll'} < 1.25(ee, e\mu)$ ($M_H = 140$ GeV) $\Delta\phi_{ll'} < 1.25(ee, e\mu)$ ($M_H = 160$ GeV) $\Delta\phi_{ll'} < 1.5(ee, e\mu)$ ($M_H = 180$ GeV) $\Delta\phi_{ll'} < 1.5(ee, e\mu)$ ($M_H = 200$ GeV)
Cut 7 H_T (scalar sum of p_T^{Jet})	$H_T < 70$ GeV

TABLE I: Summary of the selection criteria for a M_H -dependent selection in the e^+e^- and $e^\pm\mu^\mp$ final states.

A. Neural Network

The Multilayer Perceptron (MLP) neural network is used in this analysis, which is a simple feed-forward network made of neurons characterized by a bias and weighted links between them. The Neural Network used here consists of three layers, the first layer with one node per input variable, a hidden layer with one more node than input variables and a final layer with a single output node. A sigmoid function from the sum of the weighted input variables is calculated at each hidden node. The output node calculates the linear sum of these sigmoid functions with the result being close to 1 for signal-like events and close to 0 for background-like events.

In the current analysis, the neural network has been trained against the dominant background source after ‘‘Cut 7’’ (WW production) and later applied to all (background) events. Optimization of the NN has been performed for each studied Higgs mass and for e^+e^- , $e^\pm\mu^\mp$ and $\mu^\pm\mu^\mp$ channels separately. Depending on the final state and the Higgs mass, separate neural networks are constructed using kinematic variables which may be different for each Higgs mass and final state. (Five input variables are used for the NN construction in the e^+e^- and $e^\pm\mu^\mp$ channels and eight in the $\mu^+\mu^-$ final state.) Training is performed after application of kinematical pre-cuts. The list of all variables used for NN training is given below:

- the p_T of the leading lepton,
- the p_T of the next-to-leading lepton,
- the invariant di-lepton mass,
- the azimuthal angle between the two leptons,
- the missing transverse energy \cancel{E}_T ,
- the azimuthal angle between the leading lepton and \cancel{E}_T ,
- the azimuthal angle between the next-to-leading lepton and \cancel{E}_T ,
- the minimum transverse mass of the leptons and \cancel{E}_T ,

Selection criterion	Value
Cut 1 Preselection	Trigger, two muons with opposite charge $M_{\mu^1\mu^2} > 17 \text{ GeV}$ and $p_T^{\mu^1} > 20 \text{ GeV}$ and $p_T^{\mu^2} > 10 \text{ GeV}$ ($m_H = 120 \text{ GeV}$) $p_T^{\mu^1} > 20 \text{ GeV}$ and $p_T^{\mu^2} > 15 \text{ GeV}$ ($m_H = 140 \text{ GeV}$) $p_T^{\mu^1} > 25 \text{ GeV}$ and $p_T^{\mu^2} > 15 \text{ GeV}$ ($m_H = 160 \text{ GeV}$) $p_T^{\mu^1} > 25 \text{ GeV}$ and $p_T^{\mu^2} > 15 \text{ GeV}$ ($m_H = 180 \text{ GeV}$) $p_T^{\mu^1} > 25 \text{ GeV}$ and $p_T^{\mu^2} > 15 \text{ GeV}$ ($m_H = 200 \text{ GeV}$)
Cut 2 Missing transverse energy	$25 \text{ GeV} < \cancel{E}_T < 70 \text{ GeV}$ ($M_H = 120 \text{ GeV}$) $25 \text{ GeV} < \cancel{E}_T < 80 \text{ GeV}$ ($M_H = 140 \text{ GeV}$) $30 \text{ GeV} < \cancel{E}_T < 90 \text{ GeV}$ ($M_H = 160 \text{ GeV}$) $35 \text{ GeV} < \cancel{E}_T < 100 \text{ GeV}$ ($M_H = 180 \text{ GeV}$) $35 \text{ GeV} < \cancel{E}_T < 110 \text{ GeV}$ ($M_H = 200 \text{ GeV}$)
Cut 3 $\cancel{E}_T^{\text{Scaled}}$	$\cancel{E}_T^{\text{Scaled}} > 5$ (for $N_{Jet} > 0$)
Cut 4 $M_{min}^T(l, \cancel{E}_T)$	$M_{min}^T(\mu, \cancel{E}_T) > 30 \text{ GeV}$ ($M_H = 120 \text{ GeV}$) $M_{min}^T(\mu, \cancel{E}_T) > 30 \text{ GeV}$ ($M_H = 140 \text{ GeV}$) $M_{min}^T(\mu, \cancel{E}_T) > 40 \text{ GeV}$ ($M_H = 160 \text{ GeV}$) $M_{min}^T(\mu, \cancel{E}_T) > 45 \text{ GeV}$ ($M_H = 180 \text{ GeV}$) $M_{min}^T(\mu, \cancel{E}_T) > 45 \text{ GeV}$ ($M_H = 200 \text{ GeV}$)
Cut 5 Invariant mass $M_{l'l'}$	$M_{\mu^1\mu^2} < 60 \text{ GeV}$ ($M_H = 120 \text{ GeV}$) $M_{\mu^1\mu^2} < 70 \text{ GeV}$ ($M_H = 140 \text{ GeV}$) $M_{\mu^1\mu^2} < 75 \text{ GeV}$ ($M_H = 160 \text{ GeV}$) $M_{\mu^1\mu^2} < 85 \text{ GeV}$ ($M_H = 180 \text{ GeV}$) $M_{\mu^1\mu^2} < 95 \text{ GeV}$ ($M_H = 200 \text{ GeV}$)
Cut 6 Sum of $p_T^l + p_T^{l'} + \cancel{E}_T$	$60 < \Sigma p_T < 135$ ($M_H = 120 \text{ GeV}$) $70 < \Sigma p_T < 160$ ($M_H = 140 \text{ GeV}$) $80 < \Sigma p_T < 170$ ($M_H = 160 \text{ GeV}$) $90 < \Sigma p_T < 180$ ($M_H = 180 \text{ GeV}$) $90 < \Sigma p_T < 200$ ($M_H = 200 \text{ GeV}$)
Cut 7 H_T (scalar sum of p_T^{Jet})	$H_T < 60 \text{ GeV}$ ($M_H = 120 \text{ GeV}$) $H_T < 60 \text{ GeV}$ ($M_H = 140 \text{ GeV}$) $H_T < 60 \text{ GeV}$ ($M_H = 160 \text{ GeV}$) $H_T < 60 \text{ GeV}$ ($M_H = 180 \text{ GeV}$) $H_T < 50 \text{ GeV}$ ($M_H = 200 \text{ GeV}$)

TABLE II: Summary of the selection criteria for a Higgs mass M_H -dependent selection in the $\mu^+\mu^-$ final state.

- the sum of the lepton p_T and \cancel{E}_T .

Fig. 3 shows a reasonable agreement between data and MC for the Neural Network Output distributions corresponding to high statistics of (a) e^+e^- , (b) $e^\pm\mu^\mp$, (c) $\mu^+\mu^-$ Run IIa and (d) $\mu^+\mu^-$ Run IIb data samples after ‘‘Cut 1’’ (preselection). The peaks in the NN plots for the $\mu^+\mu^-$ final state correspond to the regions of phase space, which are cut out for the training by the use of kinematical pre-cuts. The corresponding distributions of the NN variable after the final selection are shown in Fig. 4 for (a) e^+e^- , (b) $e^\pm\mu^\mp$, (c) $\mu^+\mu^-$ Run IIa and (d) $\mu^+\mu^-$ Run IIb final states. The contribution of Higgs signal is shown to peak at high values of NN output, contrarily to the background.

Using the NNLL cross sections [17, 18] and branching fractions BR of 0.1072 ± 0.0016 for $W \rightarrow e\nu$ and 0.1057 ± 0.0022 for $W \rightarrow \mu\nu$, the expected number of events in the analyzed dataset for $H \rightarrow WW^* \rightarrow l^+l^- (ee, e\mu, \mu\mu)$ is $\simeq 3.7 \pm 0.05(\text{stat})$ events for a Higgs boson mass $M_H = 160 \text{ GeV}$. The expected signal for different values of the Higgs mass is given by the first line of Tables III to V for the each of the final states.

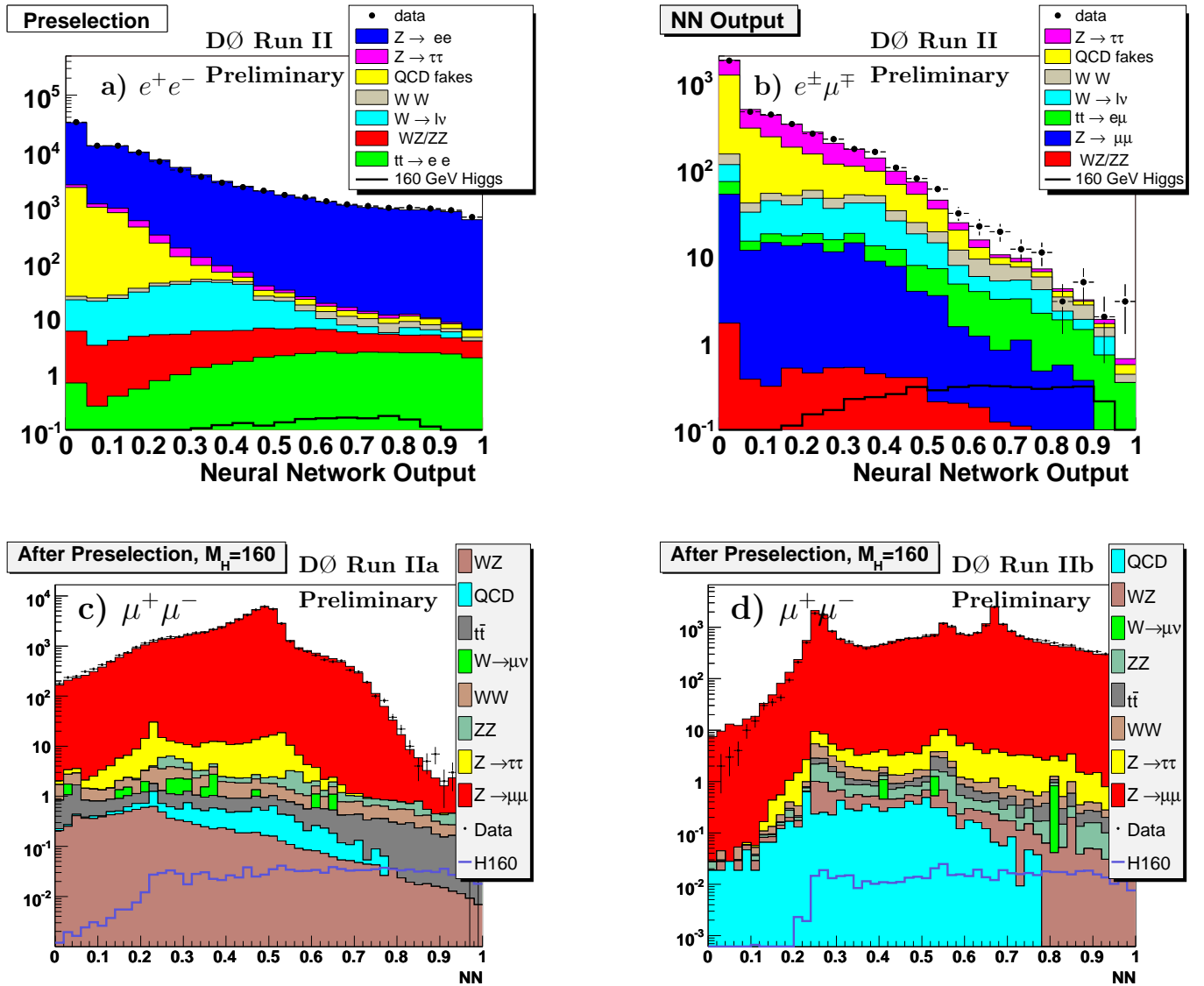


FIG. 3: Distribution of the Neural Network Output after applying the initial transverse momentum and di-lepton invariant mass cuts (“Cut 1, preselection) in the (a) e^+e^- , (b) $e^\pm\mu^\mp$, (c) $\mu^+\mu^-$ Run IIa and (d) $\mu^+\mu^-$ Run IIb final states. The expected signal for the Standard Model Higgs of mass 160 GeV is also shown.

VI. SYSTEMATICS UNCERTAINTIES

Various sources of systematic uncertainties affect the background estimation and the signal efficiency of $H \rightarrow WW^*$ production in e^+e^- , $e^\pm\mu^\mp$ and $\mu^\pm\mu^\mp$ final states: theoretical uncertainty of WW , $t\bar{t}$ and Z/γ^* production cross sections, Jet Energy Scale (JES), electron and muon reconstruction efficiencies and resolutions. In the low mass region, the uncertainty is dominated by the jet energy scale and variations in the $W + jet/\gamma$ contribution. With increasing Higgs mass, this uncertainty is decreasing because of the decreasing contribution of $W + jet/\gamma$ events. Since the WW production is the dominant background for Higgs bosons above $M_H = 160$ GeV, the systematics is dominated by the uncertainty on the WW production cross section.

For the ee and $e\mu$ final states the influence of electron and muon reconstruction efficiencies and resolutions on the background expectation is 2%. The dominant systematic uncertainty for final states including electrons is related to the JES calibration, which contributes to the uncertainty of signal ($< 5\%$) and background events (10%). For the $\mu^+\mu^-$ final state the uncertainty due to the modeling of the tail of the muon momentum resolution is 11%. The muon identification efficiency uncertainty is +8%, -5%, taken from variations in the efficiency distribution and discrepancy between Monte Carlo and data in the low mass region.

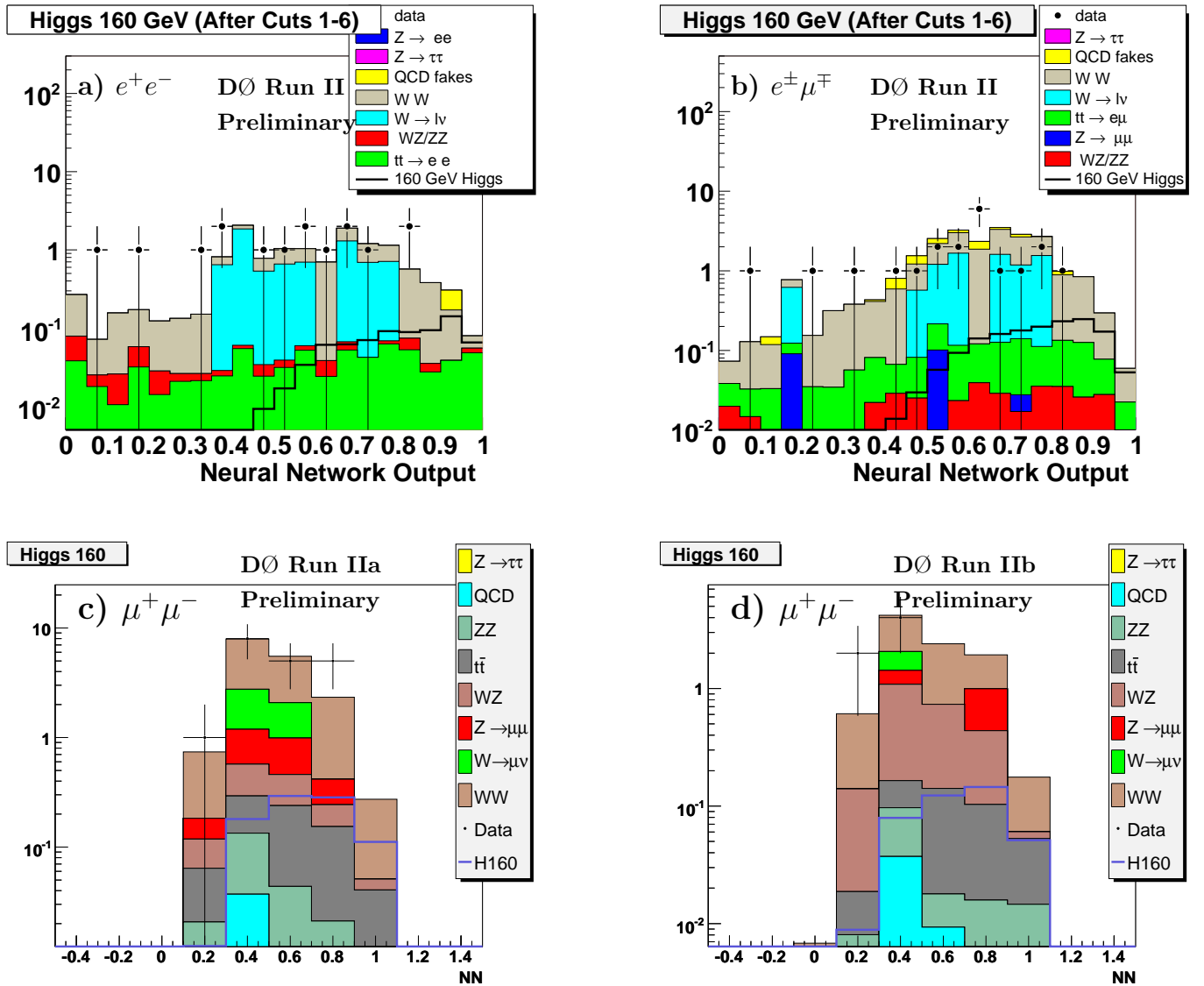


FIG. 4: Distribution of the Neural Network Output after the final selection in the in the (a) e^+e^- , (b) $e^\pm\mu^\mp$, (c) $\mu^+\mu^-$ Run IIa and (d) $\mu^+\mu^-$ Run IIb final states. The expected signal for the Standard Model Higgs of mass 160 GeV is also shown.

Finally, the theoretical cross-section uncertainty on WW production is $\sim 4\%$. The systematic uncertainty on the normalization factor is a sum of a combination of the PDF uncertainty (4%), the uncertainty on the NNLO $Z/\gamma^* \rightarrow \ell\ell$ cross section (4%) and the statistical uncertainty (2 – 4%) on the data-to-MC normalization factor. The uncertainty due to the trigger efficiency is conservatively taken to be 5%.

VII. RESULTS

A summary of the background contributions together with signal expectations and events observed in the data after the final selection is shown in the Tables III-V. Since after all selection cuts the remaining candidate events are consistent with a background observation, limits on the production cross section times branching ratio $\sigma \times BR(H \rightarrow WW^*)$ are derived for the Neural Network Analysis. Limits are calculated at 95 % confidence level using the modified frequentist CL_s approach with a Poisson log-likelihood ratio (LLR) test statistic [23]. The value of CL_s is defined as $CL_s = CL_{s+b}/CL_b$, where CL_{s+b} and CL_b are the confidence levels for the signal-plus-background hypothesis and the background-only hypothesis, respectively. The CL_s method used in this analysis utilizes the binned NN distributions (see Fig. 4) rather than simply the total number of events per channel. The expected background final

TABLE III: Number of signal and background events expected and number of events observed after all selections are applied for the e^+e^- final state using Run IIa (1.1 fb^{-1}) dataset. Only statistical uncertainties are given.

M_H (GeV)	120	140	160	180	200
$H \rightarrow W^+W^-$	0.1 ± 0.005	0.41 ± 0.03	0.78 ± 0.02	0.51 ± 0.02	0.25 ± 0.01
$Z/\gamma \rightarrow ll$	0.3 ± 0.3	0.0 ± 0.0	0.0 ± 0.0	0.3 ± 0.3	0.3 ± 0.3
Diboson (WW, WZ)	7.0 ± 0.3	7.1 ± 0.3	5.5 ± 0.3	4.3 ± 0.2	5.3 ± 0.2
t \bar{t}	1.4 ± 0.1	1.5 ± 0.1	1.4 ± 0.1	1.2 ± 0.1	1.5 ± 0.1
W +jet/ γ	5.1 ± 1.7	4.2 ± 1.5	6.7 ± 2.0	3.8 ± 1.6	5.6 ± 1.9
Multi-jet	0.2 ± 0.1	0.1 ± 0.1	0.1 ± 0.05	0.2 ± 0.1	0.15 ± 0.1
Background sum	14.1 ± 1.7	12.9 ± 1.5	13.8 ± 2.0	9.8 ± 1.6	12.9 ± 1.9
Data	12	10	15	7	11

TABLE IV: Number of signal and background events expected and number of events observed after all selection criteria are applied for the $e^\pm\mu^\mp$ final state using Run IIa (1.1 fb^{-1}) dataset. Only statistical uncertainties are given.

M_H (GeV)	120	140	160	180	200
$H \rightarrow W^+W^-$	0.21 ± 0.01	0.8 ± 0.02	1.64 ± 0.03	1.0 ± 0.03	0.7 ± 0.02
$Z/\gamma \rightarrow ll$	0.4 ± 0.2	0.2 ± 0.1	0.2 ± 0.1	0.1 ± 0.1	0.2 ± 0.1
Diboson (WW, WZ)	14.6 ± 0.1	14.2 ± 0.1	13.2 ± 0.1	10.3 ± 0.1	19.3 ± 0.1
t \bar{t}	1.1 ± 0.1	1.1 ± 0.1	1.25 ± 0.1	1.1 ± 0.1	1.9 ± 0.1
W +jet/ γ	5.5 ± 1.5	4.8 ± 1.4	7.5 ± 1.9	5.5 ± 1.6	9.9 ± 2.2
Multi-jet	1.3 ± 0.2	0.9 ± 0.2	2.1 ± 0.2	0.9 ± 0.2	1.0 ± 0.2
Background sum	23.0 ± 1.6	21.3 ± 1.5	24.2 ± 2.0	17.8 ± 1.6	32.0 ± 2.3
Data	25	20	20	14	28

distributions are smoothed via Gaussian kernel approximation to minimize any statistical fluctuations in the shape of the final variable [24]. To minimize the effect of systematics uncertainties on the search sensitivity, the individual background contributions are fitted to the data observation by minimizing a profile likelihood function, using the shape and rate of the observed distributions in the sideband regions [25]. All correlations in systematic uncertainties are maintained amongst channels and between signal and background. The resulting expected and observed upper limits are reported as a ratio of the cross section to the expected Standard Model production cross section at the NNLL order [17]. The combination of channels was performed by multiplying the individual likelihood functions of these channels resulting into a combined likelihood function.

Finally, expected and observed upper limits are reported in units of the SM production cross section times branching fraction for the combination of e^+e^- , $e^\pm\mu^\mp$ and $\mu^\pm\mu^\mp$ final states using the Run IIa dataset (1.1 fb^{-1}) and the Run IIa+Run IIb data samples (1.7 fb^{-1}).

The Run IIa combination is based on the results presented in this note. Table VI summarizes the expected (median) and observed 95% C.L. cross section for the $\sigma \times BR(H \rightarrow WW^*)$ standard model prediction. Limits are reported in units of the SM production cross section times branching fraction for e^+e^- , $e^\pm\mu^\mp$ and $\mu^\pm\mu^\mp$ final states and for combination of all three channels. Fig. 5a shows the expected and observed 95 % CL upper limit cross sections times branching ratio $\sigma \times BR(H \rightarrow WW^*)$ for the combination of e^+e^- , $e^\pm\mu^\mp$, $\mu^\pm\mu^\mp$ final states. Fig. 5b presents the

TABLE V: Number of signal and background events expected and number of events observed after all selection criteria are applied for the $\mu^+\mu^-$ final state using the combination of Run IIa (1.1 fb^{-1}) and Run IIb (0.6 fb^{-1}) datasets. Only statistical uncertainties are given.

M_H (GeV)	120	140	160	180	200
$H \rightarrow W^+W^-$	0.32 ± 0.01	0.87 ± 0.01	1.29 ± 0.01	0.90 ± 0.03	0.43 ± 0.01
$Z/\gamma \rightarrow ll$	9.4 ± 0.6	6.0 ± 0.5	1.3 ± 0.2	1.5 ± 0.2	2.9 ± 0.3
Diboson (WW, WZ)	12.5 ± 0.1	14.9 ± 0.1	9.7 ± 0.1	10.7 ± 0.1	14.7 ± 0.1
t \bar{t}	0.4 ± 0.1	0.8 ± 0.1	0.6 ± 0.1	0.7 ± 0.1	0.7 ± 0.1
W +jet/ γ	8.0 ± 1.7	3.5 ± 1.1	1.1 ± 1.1	1.0 ± 1.1	0 ± 1.7
Multi-jet	0.2 ± 0.1	0.1 ± 0.1	$0. \pm 0.$	$0. \pm 0.$	0 ± 0
Background sum	20.8 ± 1.7	25.3 ± 1.2	12.6 ± 2.0	13.8 ± 1.2	18.3 ± 1.7
Data	31	24	10	12	18

$M_H, [\text{GeV}]$	120	140	160	180	200
	expected limit (95% C.L. limit/SM (NNLL) cross section)				
ee	59.1	16.6	7.65	11.5	26.7
$e\mu$	39.9	10.7	5.0	7.2	14.8
$\mu\mu$	48.2	16.9	8.5	13.6	32.2
Run IIa combination	28.7	8.3	3.5	5.3	11.7
	observed limit (95% C.L. limit/SM (NNLL) cross section)				
ee	80.8	19.4	8.0	12.6	21.9
$e\mu$	66.3	14.9	3.7	5.7	15.7
$\mu\mu$	56.3	22.0	11.3	20.0	33.2
Run IIa combination	48.9	12.3	3.1	5.5	11.4

TABLE VI: Expected and observed upper limits at the 95% C.L. on $\sigma \times BR(H \rightarrow WW^*)$ for SM Higgs-boson production. Limits are reported in units of the SM production cross section times branching fraction for e^+e^- , $e^\pm\mu^\mp$ and $\mu^\pm\mu^\mp$ final states and for combination of all three channels using the Run IIa (1.1 fb^{-1}) dataset.

$m_h [\text{GeV}]$	120	140	160	180	200
	expected limit (95% C.L. limit/SM (NNLL) cross section)				
Run IIa combination (1.1 fb^{-1})	28.7	8.3	3.5	5.3	11.7
Run IIa + Run IIb combination (1.7 fb^{-1})	22.2	6.7	2.8	4.4	9.7
	observed limit (95% C.L. limit/SM (NNLL) cross section)				
Run IIa combination (1.1 fb^{-1})	48.9	12.3	3.1	5.5	11.4
Run IIa + Run IIb combination (1.7 fb^{-1})	47.3	12.0	2.4	4.7	11.1

TABLE VII: Expected and observed upper limits at the 95% C.L. on $\sigma \times BR(H \rightarrow WW^*)$ for SM Higgs-boson production. Limits are reported in units of the SM production cross section times branching fraction for the combination of e^+e^- , $e^\pm\mu^\mp$ and $\mu^\pm\mu^\mp$ final states in the Run IIa (1.1 fb^{-1}) and in the RunIIa+Run IIb (1.7 fb^{-1}) datasets.

log-likelihood ratio (LLR) distribution.

The Run II combination also includes Run IIb results from $e^\pm\mu^\mp$ [9] and e^+e^- [10] final states. The corresponding upper limits for the combination of Run IIa+Run IIb datasets are presented in Fig. 6a and log-likelihood ratio (LLR) distribution is shown in Fig. 6b.

Table VII summarizes 95 % CL upper limit cross sections times branching ratio $\sigma \times BR(H \rightarrow WW^*)$ for the Run IIa and the Run II (Run IIa+Run IIb) datasets in units of expected Standard Model Higgs boson production.

VIII. SUMMARY

A search for the Higgs boson is presented in $H \rightarrow WW^* \rightarrow ll'$ ($l, l' = e, \mu$) decays in $p\bar{p}$ collisions at a center-of-mass energy of $\sqrt{s} = 1.96 \text{ TeV}$. The data, collected from April 2002 to May 2007 with the Run II DØ detector, correspond to an integrated luminosity approximately $\sim 1.7 \text{ fb}^{-1}$ in the e^+e^- , $e^\pm\mu^\mp$ and $\mu^+\mu^-$ final states. The number of events observed is consistent with expectations from Standard Model backgrounds. Limits for the combination of three channels on the production cross section times branching ratio $\sigma \times BR(H \rightarrow WW^*)$ are presented in units of expected Standard Model Higgs boson production.

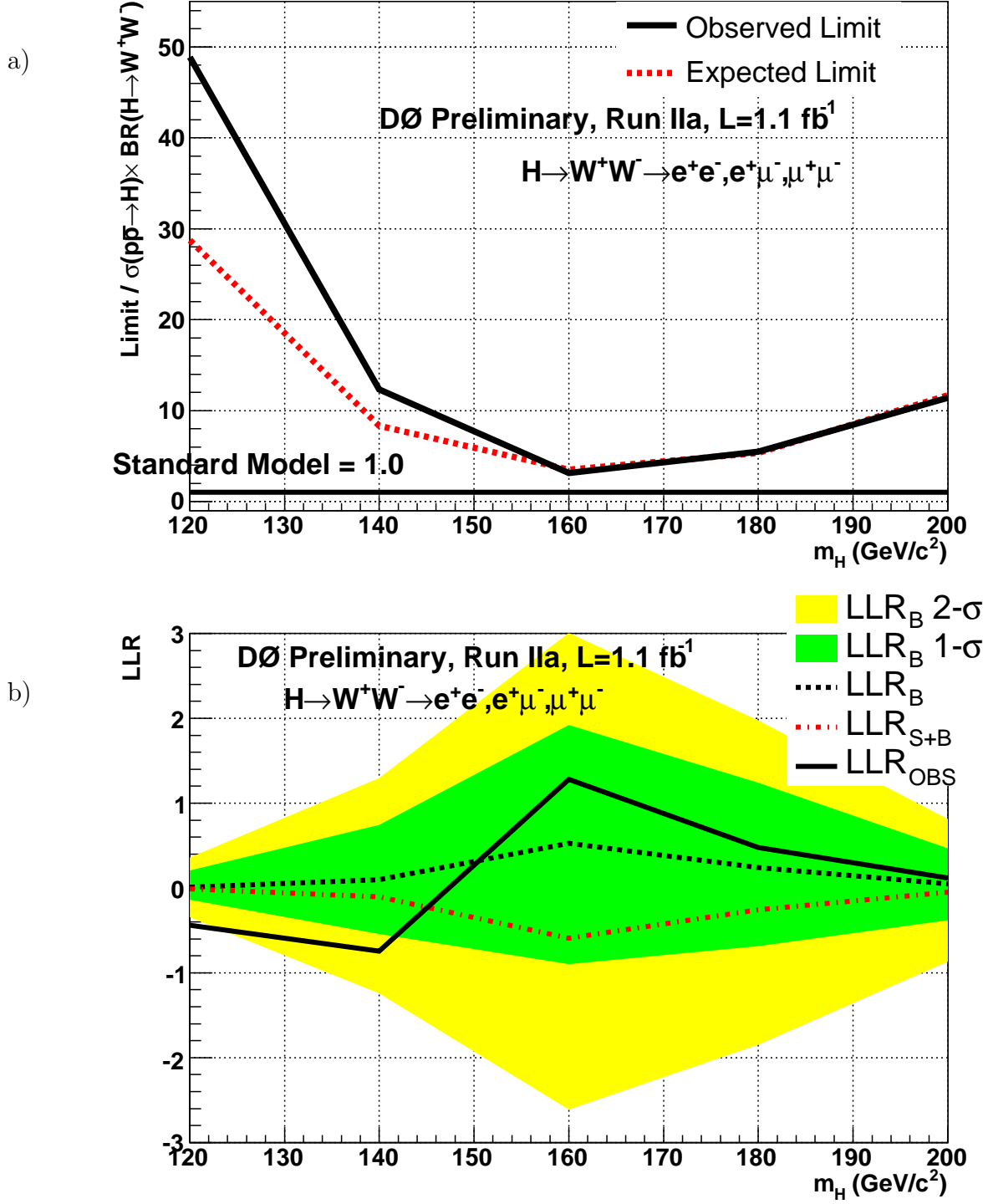


FIG. 5: a) The expected and observed 95 % CL upper limit cross sections times branching ratio $\sigma \times BR(H \rightarrow WW^*)$ in units expected Standard Model Higgs boson production for the combination of $H \rightarrow WW^* \rightarrow e^+e^-, e^\pm\mu^\mp, \mu^\pm\mu^\mp$ final states. b) Log-likelihood ratio (LLR) distribution for the combination of $H \rightarrow WW^* \rightarrow e^+e^-, e^\pm\mu^\mp, \mu^\pm\mu^\mp$ final states. The data sample used corresponds to Run IIa luminosity of 1.1 fb^{-1} . Shown in the plot are LLR_b (background-only hypothesis), LLR_{s+b} (signal+background hypothesis), LLR_{obs} (observed LLR value), and the 1- σ and 2- σ bands for the LLR_b distribution. The data sample used corresponds to Run IIa luminosity of 1.1 fb^{-1} .

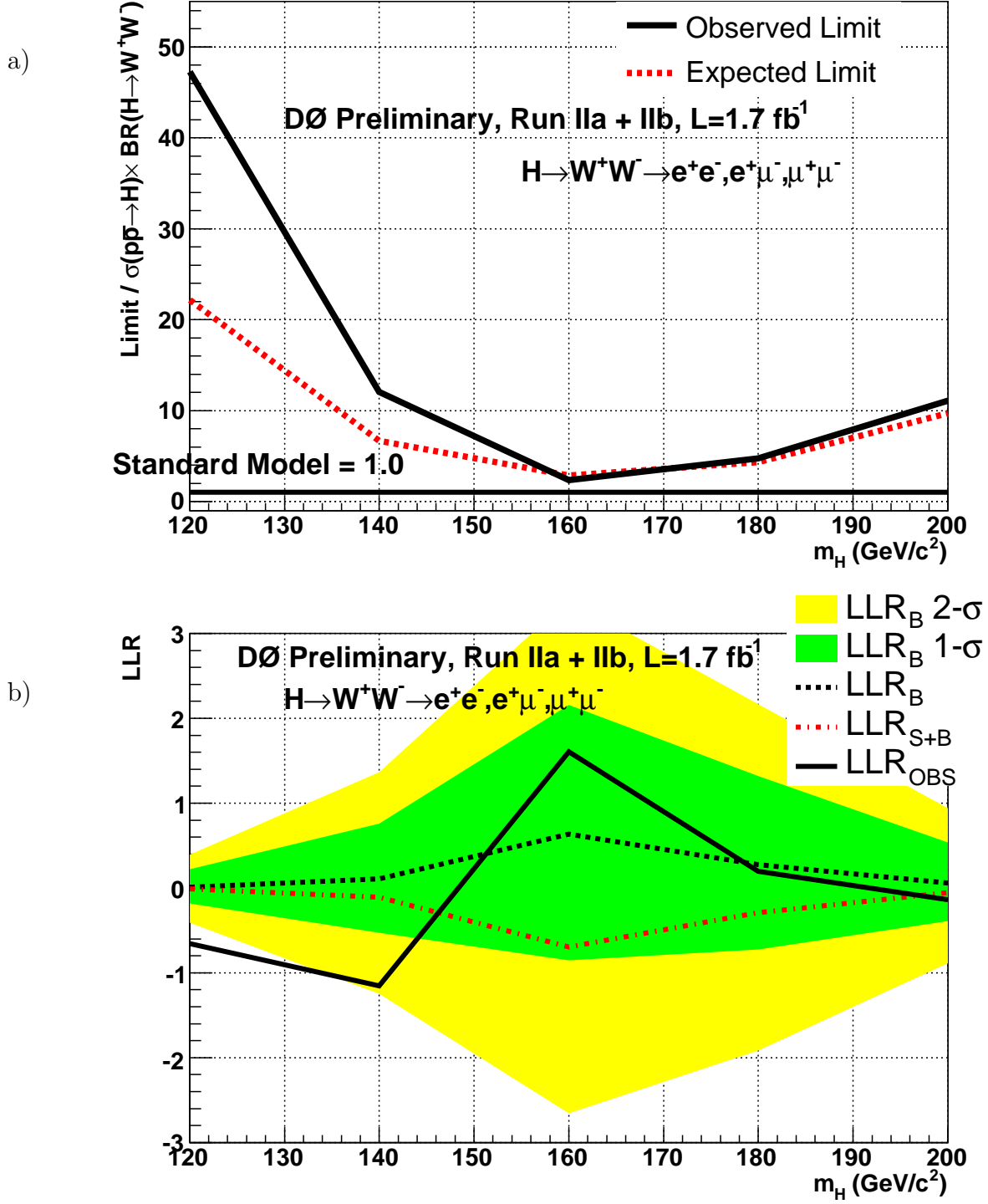


FIG. 6: a) The expected and observed 95 % CL upper limit cross sections times branching ratio $\sigma \times BR(H \rightarrow WW^*)$ in units expected Standard Model Higgs boson production for the combination of $H \rightarrow WW^* \rightarrow e^+e^-, e^\pm\mu^\mp, \mu^\pm\mu^\mp$ final states. b) Log-likelihood ratio (LLR) distribution for the combination of $H \rightarrow WW^* \rightarrow e^+e^-, e^\pm\mu^\mp, \mu^\pm\mu^\mp$ final states. Shown in the plot are LLR_b (background-only hypothesis), LLR_{s+b} (signal+background hypothesis), LLR_{obs} (observed LLR value), and the 1- σ and 2- σ bands for the LLR_b distribution. The results correspond to the Run II dataset of 1.7 fb^{-1} .

-
- [1] R. Barate *et al.*, Phys. Lett. B **565**, 61 (2003).
 - [2] The LEP Collaborations, the LEP Electroweak Group, the SLD Electroweak and Heavy Flavours Group, “A combination of preliminary electroweak measurements and constraints on the standard model,” arXiv:hep-ex/0612034.
 - [3] T. Han, A. Turcot, R-J. Zhang, Phys. Rev. D. **59**, 093001 (1999).
 - [4] M. Carena *et al.*, “Report of the Tevatron Higgs working group”, arXiv:hep-ph/0010338.
 - [5] K. Jakobs, W. Walkowiak, ATLAS Physics Note, ATL-PHYS-2000-019.
 - [6] J. Elmsheuser, M. Hohlfeld, Phys. Rev. Lett. **96**, 011801 (2006).
 - [7] DØ Collaboration, DØ Note 5194-CONF.
 - [8] DØ Collaboration, DØ Note 5063-CONF.
 - [9] DØ Collaboration, DØ Note 5489-CONF.
 - [10] DØ Collaboration, DØ Note 5502-CONF.
 - [11] DØ Collaboration, DØ Note 5504-CONF.
 - [12] DØ Collaboration, V. Abazov *et al.*, Nucl. Instrum. Meth. A **565**, 463 (2006).
 - [13] DØ Collaboration, S. Abachi *et al.*, Nucl. Instrum. Methods Phys. Res. A **338**, 185 (1994).
 - [14] V. Abramov *et al.*, Nucl. Instrum. Meth. A **419**, 660 (1998).
 - [15] T. Sjöstrand *et al.*, Comp. Phys. Comm. **135**, 238 (2001).
 - [16] R. Brun and F. Carminati, CERN Program Library Long Writeup W5013, 1993 (unpublished).
 - [17] S. Catani, D. Florian, M. Grazzini, P. Nason, JHEP **07**, 028 (2003) [hep-ph/0306211].
 - [18] S. Catani, D. Florian, M. Grazzini, JHEP **01**, 015 (2002).
 - [19] A. Djouadi *et al.*, Comput. Phys. Commun. **108**, 56 (1998).
 - [20] R. Hamberg, W.L. van Neerven, and T. Matsuura, Nucl. Phys. **B359** 343 (1991) [Erratum-ibid. **B644** 403 (2002)].
 - [21] N. Kidonakis and R. Vogt, Phys. Rev. D **68**, 114014 (2003).
 - [22] J. M. Campbell and R. K. Ellis, Phys. Rev. D **60**, 113006 (1999).
 - [23] T. Junk, Nucl. Instr. and Meth., **A434**, 435 (1999)
 - [24] K.S. Cranmer, Comput. Phys. Commun., **136**, 198 (2001) [arXiv:hep-ph/0011057].
 - [25] W. Fisher, “Systematics and Limit Calculations”, FERMILAB-TM-2386-E.
 - [26] E. Arik *et al.*, Acta Phys. Polon. B **37**, 2839 (2006) [arXiv:hep-ph/0502050].
 - [27] E. Arik *et al.*, Eur. Phys. J. C **26**, 9 (2002).